Inline ECE measurements for NTM control on ASDEX Upgrade

H. van den Brand[1,2], W.A. Bongers[1], J.K. Stober[3], W. Kasparek[4], D. Wagner[3], N. Doelman[5,6], W. Klop[5], L. Giannone[3], M. Reich[3], E. Westerhof[1], M. R. de Baar[1,2], the ASDEX Upgrade team[3] & the EUROfusion MST1 team[7]

[1] FOM Institute DIFFER - Dutch Institute for Fundamental Energy Research, P.O. Box 6336, 5600 HH Eindhoven, The Netherlands

[2] Control Systems Technology Group, Department of Mechanical Engineering, Eindhoven University of Technology, P.O. Box 513, 5600 MB Eindhoven, The Netherlands

[3] Max Planck Institut für Plasmaphysik, Boltzmannstraße 2, 85748 Garching bei München, Germany

[4] Institut für Grenzflächenverfahrenstechnik und Plasmatechnologie, Universität Stuttgart, Pfaffenwaldring 31, D-70569 Stuttgart, Germany

[5] Department of Opto-Mechatronics, TNO Technical Sciences, Stieltjesweg 1, 2628 CK Delft, The Netherlands

[6] Leiden Observatory, University of Leiden, Niels Bohrweg 2, 2333 CA Leiden, The Netherlands

[7] See the author list H. Meyer *et al* 2017 Nucl. Fusion 57 102014

E-mail: `H.vandenbrand@differ.nl`

Abstract. The successful use of a tokamak for generating fusion power requires an active control of magnetic instabilities, such as neoclassical tearing modes (NTMs). Commonly, the NTM location is determined using electron cyclotron emission (ECE) and this is used to apply electron cyclotron heating (ECH) on the NTM location. In this paper, an inline ECE set-up at ASDEX Upgrade is presented in which ECE is measured and ECH is applied via the same path. First results are presented and a means to interpret the measurement data is given. Amplitude and phase with respect to a reference magnetic signal are calculated. Based on the amplitude and phase, the time of mode crossing is determined and shown to compare well with real-time estimates of the mode crossing time. The ECH launcher and flux surface geometries at ASDEX Upgrade, which are optimized for current drive by a beam path that is tangential to the flux surface near deposition, make it difficult to identify the mode crossing without inline ECE launcher movement. Therefore, NTM control based on inline ECE requires launcher movement to determine and maintain a reliable estimate of the NTM location.

Submitted to: *Nucl. Fusion*

1. Introduction

In tokamak plasmas, the need for control of MHD instabilities is growing with the size of the tokamak, as the impact of the instabilities increases and becomes more and more detrimental [1]. The neoclassical tearing mode (NTM) is particularly limiting as it decreases confinement and could induce a disruption, a violent termination of the fusion plasma [2]. Electron Cyclotron Heating (ECH), which consists of Electron cyclotron current drive (ECCD) and electron cyclotron resonance heating (ECRH) depending on the toroidal angle of the ECH beam, has proved its usefulness in suppressing magnetic islands [3, 4].

Closed-loop control of NTMs is demonstrated in multiple tokamaks, e.g. ASDEX Upgrade [5], DIII-D [6, 7], and TEXTOR [8]. The two most common approaches for control of NTMs are i) measuring the NTM location with electron cyclotron emission (ECE) and relating this to ECH launcher settings and ii) minimizing a quantity, such as the island width, by systematically moving the ECH launcher. These approaches have proved to be fruitful at ASDEX Upgrade and DIII-D [5, 6, 7]. Hennen *et al* exploited the similar nature of ECE and ECH to measure via the same transmission line and use this signal for control [9, 10, 8]. The advantage of using the measurement technique used by Hennen *et al* is that a direct feedback on the mode location, determined solely by ECE, is possible, without a need to incorporate additional measurements and real time ray-tracing. However, the TEXTOR tokamak presents a limited test case for reactor-relevant NTM control, as only L-mode plasmas were available, NTMs are seeded by external coils, the shape is circular instead of D-shaped, and the ECH system at TEXTOR consisted of quasi-optical transmission lines, which is different from the waveguide transmission lines proposed for ITER. Therefore, the results obtained by Hennen *et al* are not sufficient for direct comparison with the results in more reactor-relevant tokamaks such as ASDEX Upgrade, DIII-D, and ITER. Due to the changes, NTM size could be different and separation of ECH and ECE needs a different design. Detection and control of NTMs with inline ECE should therefore be validated in a more reactor-relevant environment. In this paper, such reactor-relevant inline ECE measurements (i.e. ECE measurements in an ECH transmission line) at ASDEX Upgrade are presented.

The set-up for inline ECE measurements (as developed by Bongers *et al* [11]) and a means to interpret the uncalibrated measurements are presented. The key features of these measurements are discussed. The lock-in amplification technique (see Reich *et al* [12]) is used to determine the correlation amplitude and phase of inline ECE measurements with respect to magnetic measurements and hence, the location of the NTMs based on the inline ECE measurements.

This paper is organized as follows: In the next section, the experimental set-up for inline ECE measurements at ASDEX Upgrade is introduced. Section 3 discusses the measurements that are made with the inline ECE radiometer and presents two of the main characteristics of the measurement data. In section 4, the crossing time of NTMs is determined using inline ECE and compared with crossing times derived from

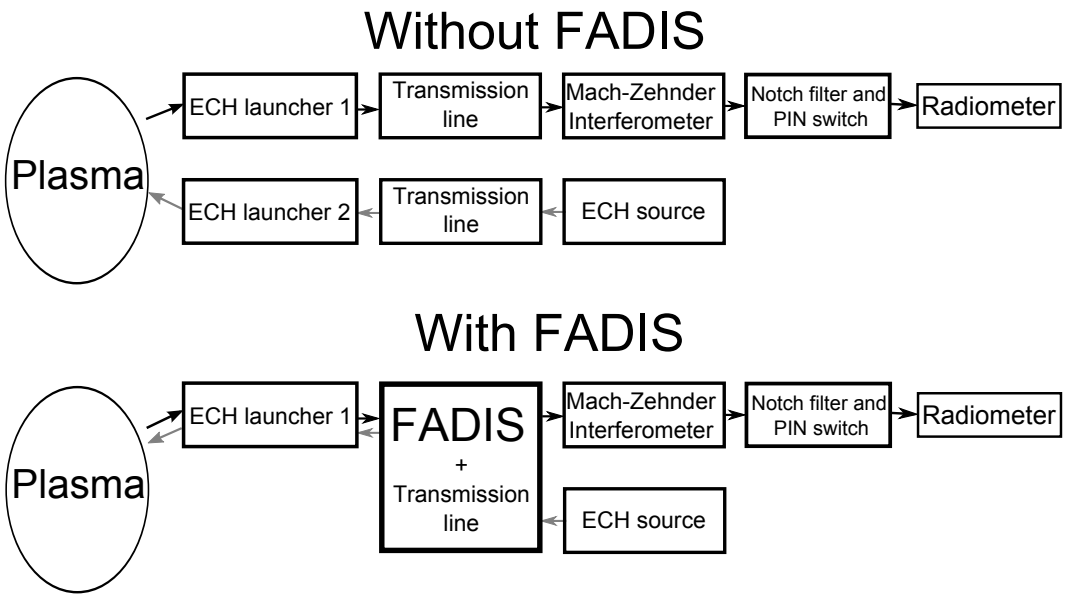

Figure 1. Schematic drawing of the inline ECE set-up [13], with the following components: radiometer, Bragg reflector notch filter and PIN switch, Mach-Zehnder interferometer, ECH launcher, and plasma. The figure shows a configuration without FADIS (top), which has been used for commissioning purposes, and the final configuration with FADIS (bottom) as intended for use in NTM control. Black arrows indicate the path of ECE from plasma to the radiometer. Grey arrows indicate the ECH radiation, which could be supplied through FADIS. Only one of the two FADIS output ports at the plasma side is shown. The specific configurations used in different experiments are discussed in Subsection 2.4.

other diagnostics. Using inline ECE for real-time control is discussed in section 5 and concluding remarks are given in section 6. This paper is based on Chapter 4 of the PhD thesis of the first author [13].

2. Inline ECE set-up at ASDEX Upgrade

Inline ECE measurements are made with a six-channel heterodyne radiometer, which is described in Subsection 2.1. Both an ECH source and the inline ECE radiometer are connected to one of the ECH launchers of the ASDEX Upgrade ECH system [14]. ECH radiation at 140 GHz and ECE coming from the plasma are split using the FAst DIrectional Switch (FADIS) [15], of which the main characteristics for inline ECE are given in subsection 2.2. ECH radiation, with power levels up to 4 MW, could inflict permanent damage to the radiometer, which requires power levels below 1 mW. A Mach-Zehnder interferometer, a Bragg reflector notch filter and a PIN switch, described in Subsection 2.3, protect the radiometer against high power ECH radiation. Various configurations have been used for connecting the inline ECE set-up to the ECH launcher, which are described in Subsection 2.4. An overview of the different inline ECE components is shown in figure 1.

2.1. Heterodyne radiometer

A six-channel heterodyne radiometer is used for the inline ECE measurements [16]. The radiometer has an internal mixer and a local oscillator at 126.6 GHz and an image rejection filter (high-pass at 125 GHz). Six Schottky diodes detect the downconverted ECE around the central channel frequencies $f_1 = 132.5$ GHz, $f_2 = 135.5$ GHz, $f_3 = 138.5$ GHz, $f_4 = 141.5$ GHz, $f_5 = 144.5$ GHz, and $f_6 = 147.5$ GHz. For ASDEX Upgrade discharges 31059 and lower, an intermediate frequency bandwidth of 500 MHz is used, while for discharges 31953 and higher, the bandwidth is set to 1.5 GHz. The radial resolution of radiometer channels is a function of the radiometer characteristics, the plasma conditions, and the measurement line-of-sight through the plasma. Therefore, the measurement resolution is addressed in a later section. Each channel is equipped with a first order low pass filter with a video bandwidth of 100 kHz for ASDEX Upgrade discharges up to 31059, and 30 kHz for ASDEX Upgrade discharges 31060 and higher. Additionally, each channel has two potentiometers for offset correction and gain adjustment, respectively. The output voltage of each channel ranged between 0 V and 10 V for ASDEX Upgrade discharges up to 31059, and between -1.2 V and +1.25 V for ASDEX Upgrade discharges 31060 and higher. In this paper, measurements are shown with both these voltage ranges. The data of the six radiometer channels is sampled at 400 kHz on a data acquisition unit of which the clock should be synchronized with the ASDEX Upgrade timing system. The time synchronization allows a comparison of the inline ECE measurements with the other ASDEX Upgrade signals. For the discharges 31967 to 32556 presented in this paper there were problems with this time synchronization of the data acquisition unit with the ASDEX Upgrade timing system. For discharges 31967, 31978, and 31986 the timing is corrected before the correlation is applied.

2.2. Fast directional switch for inline ECE

The FAst DIrectional Switch (FADIS) Mk II is present at the ASDEX Upgrade ECH system [15]. FADIS is a bi-directional diplexer with four ports and can be mounted in two transmission lines. For clarity, we will designate the ports on the plasma side as 'output ports' and the ports on the ECH system and inline ECE radiometer side as 'input ports'. FADIS is a ring-resonator with two fixed corrugated mirrors and two focussing resonator mirrors of which one is movable such that the resonance frequency of FADIS can be controlled [17]. For a given input port of FADIS, one of the output ports has a peak in the transmission and is known as the resonant output port, while the other output port has a notch characteristic and is known as the non-resonant output port. For inline ECE, FADIS is, at the plasma side, connected to two ECH launchers and at the ECH system side it is connected to the inline ECE set-up and an ECH source. By choosing the resonance frequency of FADIS equal to the ECH frequency, the non-resonant frequencies entering from the plasma side through the ECH output port are passed to the inline ECE set-up, while the ECH frequency is suppressed.

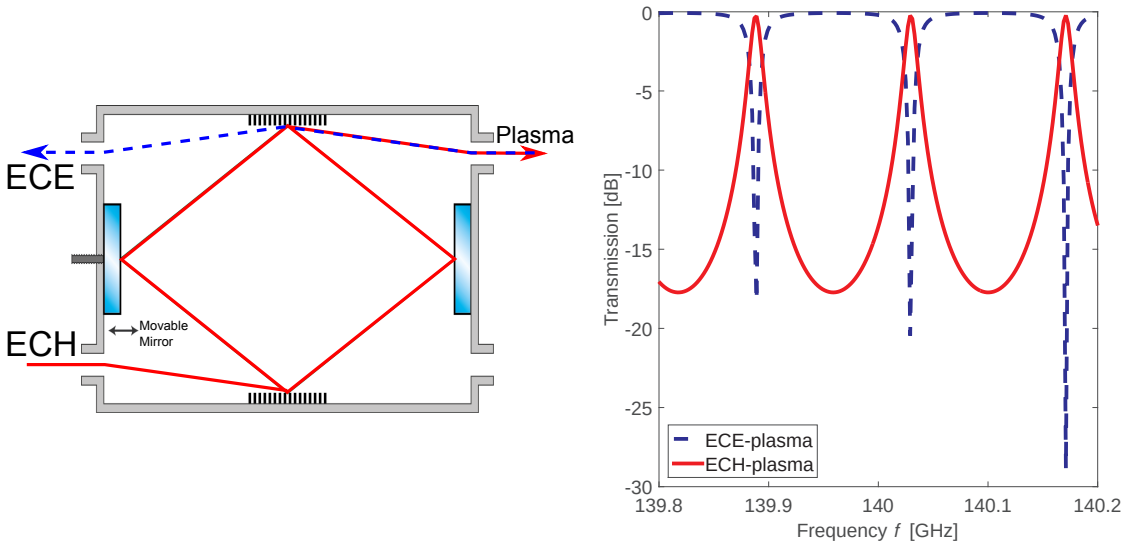

Figure 2. Schematic overview of the bi-directional FADIS set-up on the left [13], which shows two output ports on the plasma side (right) and two input ports (left), connected to the inline ECE radiometer and an ECH source. The paths traveled by ECH and ECE are indicated in red and blue, respectively. Grated mirrors are visible at the top and bottom of FADIS. Two resonator mirrors are shown at the left and right. The left mirror is used to adjust the resonance frequency. The transmission as a function of frequency is shown on the right, for the paths traveled by ECH and ECE in red and blue, respectively, which are the resonant and non-resonant ports for the port labeled plasma. Note that the transmission can be varied by changing either the frequency or the position of the FADIS movable mirror. Residual ECH power, which is not transmitted via the resonant port to the plasma, is dumped into a load connected to the open port (not shown).

Figure 2 shows a schematic overview of the coupling of radiation of the FADIS set-up and indicates that a maximum suppression of 25 dB for the HE_{11}-mode of the ECH radiation entering the inline ECE set-up can be reached using FADIS. In practice, the ECH radiation entering FADIS from the plasma consists of a mixture of multiple modes. The intensity is expected to be far below 10 % of the incident radiation due to ECH absorption in the plasma. A suppression of 40 dB for multi-mode radiation is measured for FADIS Mk II [18]. As a result, a 50 dB suppression of ECH radiation by FADIS is expected. Additionally, figure 2 shows that a part of the ECE radiation is filtered by FADIS. Due to this filtering, the collected ECE radiation is reduced by about 15 %.

2.3. ECH radiation suppression using Mach-Zehnder interferometer, notch filter, and PIN switch

The ECH installed power, at the moment of measurement, was 4 MW, while a radiation level in excess of 1 mW severely damages the six-channel radiometer. Therefore, ECH radiation needs to be reduced by a factor of 90 dB in order not to damage the radiometer. The ECH sources at ASDEX Upgrade routinely operate at 140 GHz and occasionally

provides radiation at 105 GHz. Therefore, the suppression of 90 dB is assured for radiation at 140 GHz, while the inline ECE set-up is not used for 105 GHz ECH operation. An even larger suppression of 110 dB is needed to ensure that inline ECE measurements are possible [10]. A 30 dB suppression is achieved using the Mach-Zehnder interferometer over a frequency range of 500 MHz centered around 140 GHz [19]. Closer to 140 GHz, a suppression of up to 50 dB is reached. The over-sized Mach-Zehnder is used to limit the power in the connected waveguides and thereby prevents arcing. A Bragg reflector notch filter is used for additional suppression [20]. This filter suppresses 140 GHz by 60 dB and 105 GHz radiation by 55 dB. Therefore, together with the 50 dB suppression by FADIS, a suppression of 140 dB is reached for 140 GHz. However, it is known that at the start of ECH the frequency is about 200 MHz from 140 GHz and therefore not within the notch of FADIS. To protect the radiometer during ECH start, a PIN switch is used to block the transmission line when a trigger signal is provided and this results in 45 dB suppression for the entire frequency range. If FADIS is not tuned for 140 GHz suppression, the achieved suppression around 140 GHz is 135 dB with PIN switch and 90 dB without the PIN switch.

2.4. Connection of the ECE set-up to the ASDEX Upgrade tokamak

During this commissioning phase of the inline ECE set-up, it has been used in various different configurations. A schematic overview of the different ECE set-ups, connected with and without FADIS, is shown in figure 1. In the inline ECE set-up radiation always enters the radiometer via the Mach-Zehnder interferometer. In the final inline ECE set-up, as intended for use in NTM control, it is connected via the FADIS set-up. On the plasma side, FADIS is connected to two ECH launchers of which one corresponds to the resonant channel for the ECH source. This is also the output port through which most ECE is collected using the non-resonant channel and, therefore, this is the only ECH launcher shown in the bottom part of figure 1. There have been measurements both with and without an ECH source connected to FADIS. FADIS is equipped with two polarizers which are set to match the polarization for second harmonic X-mode for a given magnetic field and plasma current. In this configuration the available ECH power is limited to 2 MW out of 4 MW due to i) a disconnected gyrotron that is replaced by inline ECE and ii) a power reduction of the gyrotrons to prevent arcing in FADIS and the non-evacuated transmission lines.

For part of the discharges used for commissioning of the diagnostic, the inline ECE set-up is directly connected to one of the ECH launchers. More recently, a waveguide switch and two polarizers have been used in one of the ECH system transmission lines, such that one can switch in-between discharges from ECH heating to inline ECE measurements. Table 1 indicates the discharge ranges in which a particular configuration is used and lists particular discharges of which data is shown in this paper.

Table 1. Overview of the different configurations in which the inline ECE set-up is used. The last column indicates the discharges in this paper that are done with the specified configuration.

Configuration	Discharges with this configuration	Discharges in this paper
FADIS with ECH	27792-27812,29517-29592	27808,29569
FADIS without ECH	29949-30021	
Direct connection to transmission line	29106-29126,31038-31059	31045
Waveguide switch	31953-32003,32498-32561	31967,31978 31989

3. Main characteristics of inline ECE measurements

Inline ECE measurements are done in multiple ASDEX Upgrade discharges as is indicated by table 1. In these discharges, the inline ECE set-up produces six voltage signals as a function of time, which are uncalibrated. Subsection 3.1 discusses how the results from the TORBEAM code can be used to interpret the quality of the measurements. Most measurements include ECH, which leads to spikes on the inline ECE measurements. Subsection 3.2 discusses the spikes that are observed during ECH.

3.1. Measurement interpretation using TORBEAM

The inline ECE measurement location depends on the launcher settings. This is both a great asset and a complication for interpreting the six uncalibrated voltage signals. The TORBEAM code is used as a tool for interpreting the measurements [21]. With this code, the location of maximum power deposition $\rho_{dep,max}(f)$ is calculated for an EC frequency f and for given plasma conditions and launcher settings. In this paper, ρ is the normalized poloidal flux. For both ECE and ECH, the resonance locations are the same. The normalized power deposition profile is, however, in general not equal to the birthplace distribution of observed ECE intensity [22]. Only for a constant temperature over the power deposition and emission region and for a constant ratio between the emission volume and flux surface volume is the normalized power deposition profile equal to the birthplace distribution of observed intensity.

In this paper, the deposition location of ECH power is given by $\rho_{ECH} = \rho_{dep,max}(140\text{ GHz})$. The measurement location of an inline ECE measurement for channel i is approximated by $\rho_{IEC,i} = \rho_{dep,max}(f_i)$, with f_i as defined in subsection 2.1. This approximation only holds for a constant temperature near the deposition location and for a constant ratio between the emission volume and flux surface volume. The top plot of figure 3 shows the peak emission locations in solid lines for inline ECE channels 1, 2, and 3 (denoted as IEC1 to IEC3, respectively). In discharge 31045, the inline ECE launcher is set for a perpendicular view with toroidal angle $\phi = 0°$ at a

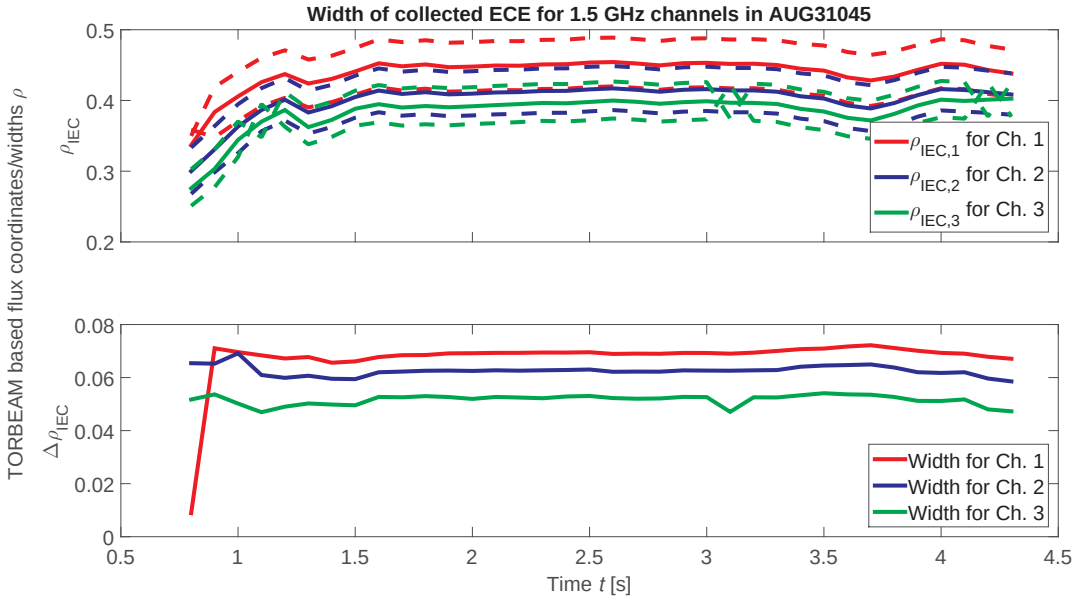

Figure 3. Emission locations for three inline ECE channels (top plot) and width of emission region (bottom plot) for discharge 31045 [13]. The top plot shows the peak emission locations at the central frequency of each channel as a solid line and the locations of 6dB points of the emission profiles at the ±750 GHz frequency edges of the channel with dashed lines. The inline ECE launcher is set to a perpendicular view with toroidal angle $\phi = 0°$ at a magnetic field of -2.5 T and a plasma current of 800 kA.

magnetic field of -2.5 T and a plasma current of 800 kA. The width of the emission profiles is assessed by evaluating the emission at the channel centre frequencies plus half the channel width, $f_{w,i} = f_i \pm 750$ MHz, adding the 6 dB width of the intrinsic emission profile at that frequency. The top plot shows that if the width of the channels is considered, inline ECE channel 2 overlaps fully with ranges that are already covered by inline ECE channels 1 and 3. The width of the emission region for the three channels is shown in the bottom plot figure 3. Note that the width of the three depicted channels is between $\Delta\rho_{IEC} = 0.05$ and $\Delta\rho_{IEC} = 0.07$. Therefore, a portion of at least 1/20 of the minor radius is covered by a single channel.

Figure 3 shows the emission locations and widths for a constant launcher angle. However, the usefulness of inline ECE stems from the possibility to vary the measurement locations. At a fixed toroidal launcher angle of $\beta = -7.7°$, the poloidal launcher angle is changed, which results in a combined change of both the poloidal angle θ and toroidal angle ϕ, and, hence, a changing deposition location. Most 3/2 NTM scenarios use a magnetic field of -2.6 T and plasma current of 1 MA. For the toroidal launcher angle $\beta = -7.7°$, the toroidal and poloidal injection angles are varied from $\phi = -11°$ and $\theta = -6°$ to $\phi = -8°$ and $\theta = 14°$. Figure 4 shows the location of the six inline ECE channels for $\theta = 5°$ and $\phi = -9°$ for a typical 3/2 NTM ASDEX Upgrade discharge.

Figure 5 shows discharge 31978 in which the launcher is swept twice over the mode

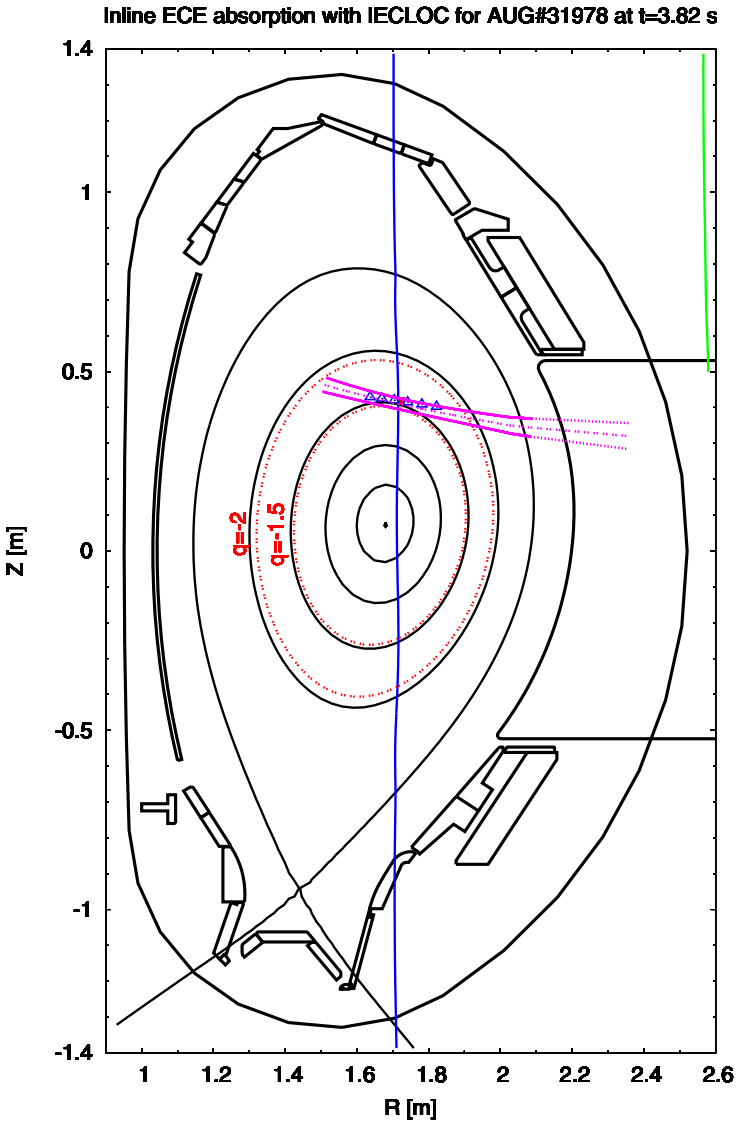

Figure 4. Poloidal cross section for ASDEX Upgrade discharge 31978 at 3.82 s [13]. Black lines in the plasma vessel indicate the poloidal flux surfaces for $\rho = \{0.2, 0.4, 0.6, 0.8, 1.0\}$. The $q = 3/2$ and $q = 2$ flux surfaces are indicated by red dashed lines. The locations of absorption for radiation with frequencies f_i, corresponding to inline ECE channels i, are indicated by blue triangles. The absorption location for 140 GHz radiation is noted by a red dot. The second harmonic resonance is indicated by a blue vertical line. The beam path is indicated by a magenta line. The inline ECE launcher is set for NTM suppression with $\beta = -7.7°$ at a magnetic field of -2.6 T and a plasma current of 1 MA.

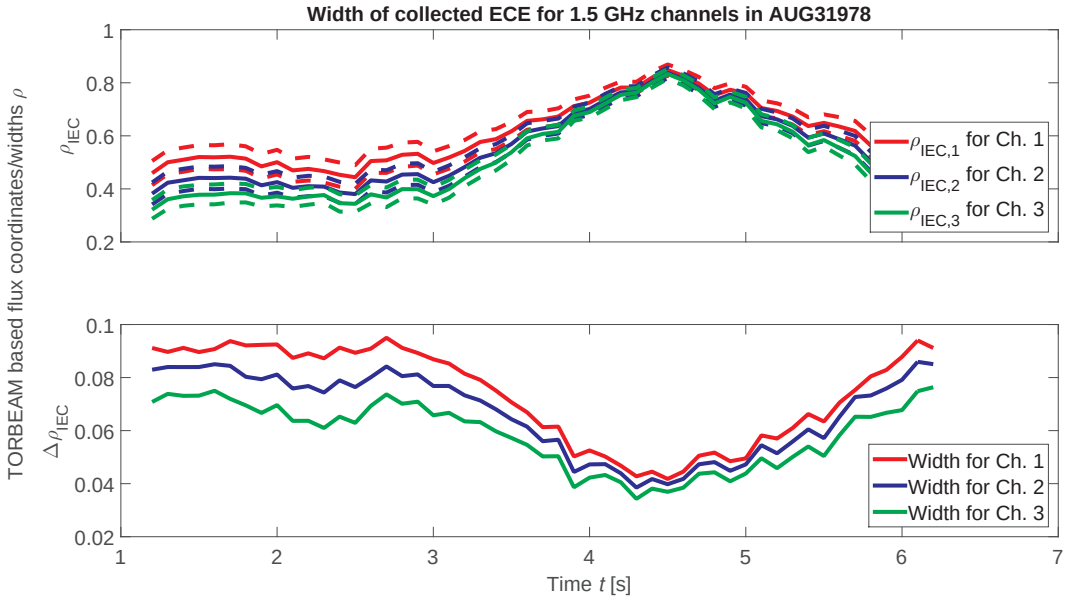

Figure 5. Emission locations for three inline ECE channels (top plot) and width of emission region (bottom plot) for discharge 31978, in which the launcher moved [13]. The top plot shows the peak emission locations at the central frequency of each channel as a solid line and the locations of 6dB points of the emission profiles at the ±750 GHz frequency edges of the channel with dashed lines. The inline ECE launcher is set for NTM suppression with $\beta = -7.7°$ at a magnetic field of -2.6 T and a plasma current of 1 MA.

location with toroidal launcher angle $\beta = -7.7°$. The figure shows the emission location (as determined from the power deposition locations) and the width of the emission region. Similar to discharge 31045, a large overlap of the inline ECE channels is visible. Furthermore, the width of the emission region reduces as the emission locations move outward. This is caused by the trajectory of ECE from the emission location to the launcher, which becomes more tangential to flux surfaces for larger ρ. Consequently, for an equal emission width in centimetre, a smaller emission region $\Delta\rho_{IEC}$ is found.

The inline ECE measurements are not calibrated, but the measured voltages are expected to be linear with ECE intensity [16]. A relative calibration of inline ECE measurements can be achieved by considering the temperature at the emission location, as is derived above. The electron temperature at the emission locations is obtained from the integrated data analysis (IDA) diagnostic [23]. For every inline ECE channel, the average temperature (obtained from IDA) is divided by the average measured voltage to obtain an approximate scaling factor η_i for eV/V for each inline ECE channel. The scaling factor can be used to determine the temperature from the inline ECE voltages.

For discharge 31978, the temperatures, based on IDA, are compared with the inline ECE voltage times the scaling factor η_i for each channel i and the results are shown in figure 6. The scaling factor is determined over a time interval from 2.65 s to 2.97 s. The figure shows that an approximate scaling of the temperature measurements is achieved,

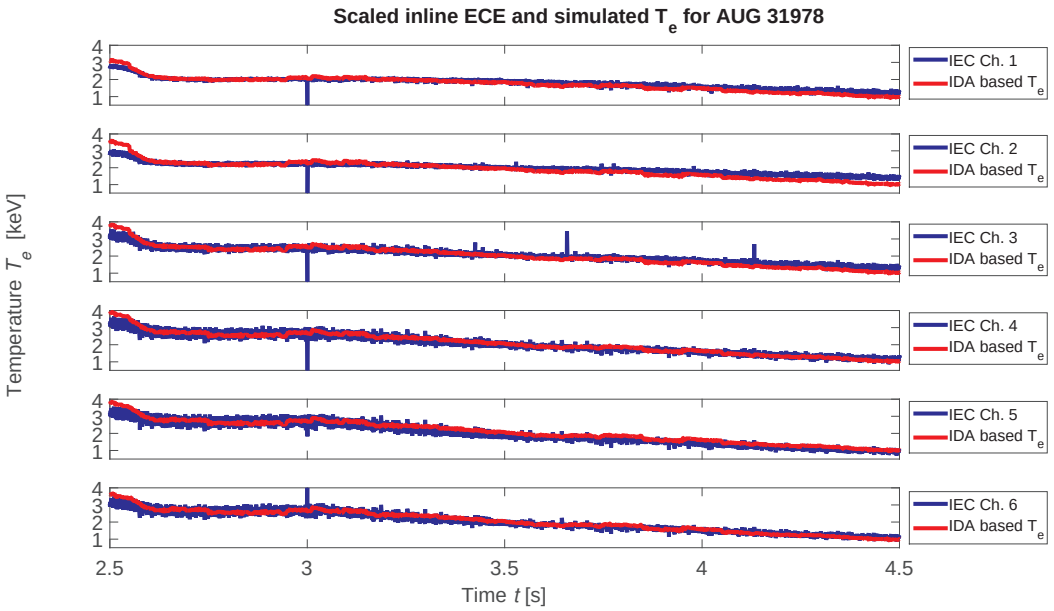

Figure 6. IDA based temperature (red), at inline ECE emission locations, compared with scaled inline ECE measurements (blue) for the six measurement channels [13]. A relative calibration of the inline ECE measurements is calculated over the time interval from 2.65 s to 2.97 s.

even when the launcher is sweeping from $\rho_{ECH} = 0.35$ at 3 s to $\rho_{ECH} = 0.8$ at 4.5 s. Scaling factors on the order of a few mV per eV are found, which corresponds to the radiometer sensitivity, which is on the order of V/eV, and an overall transmission loss in the system of 30 dB.

3.2. Measurements during ECH

Using FADIS, inline ECE could be used to measure ECE near the ECH deposition location, while simultaneously applying heating via the same transmission line. This does require that the inline ECE signals are still useful when ECH is active. Figure 7 shows a measurement of discharge 27808 in which the measurements of the six inline ECE channels are shown. During ECH via FADIS (blue) spikes on all inline ECE channels are shown. Such spikes have also been observed in discharges where FADIS is not used. In all discharges where spikes occurred, ECH is applied via a launcher close to the launcher used for inline ECE. The spikes occur mostly in H-mode discharges and seem to be related to magnetic instabilities such as the sawtooth and edge-localized modes (ELMs) as is shown figure 8, which contains a zoom of the six inline ECE channels, shown in figure 7, between 4.2 s and 4.3 s [24].

The bottom plot of figure 8 shows the divertor current, which shows a dip when an ELM occurs. In each plot, the occurrence of ELMs is shown using grey boxes. ELMs and the associated dips in the divertor current correspond with spikes on the inline ECE measurement channels. Additionally, there are a few time points for which a spike on

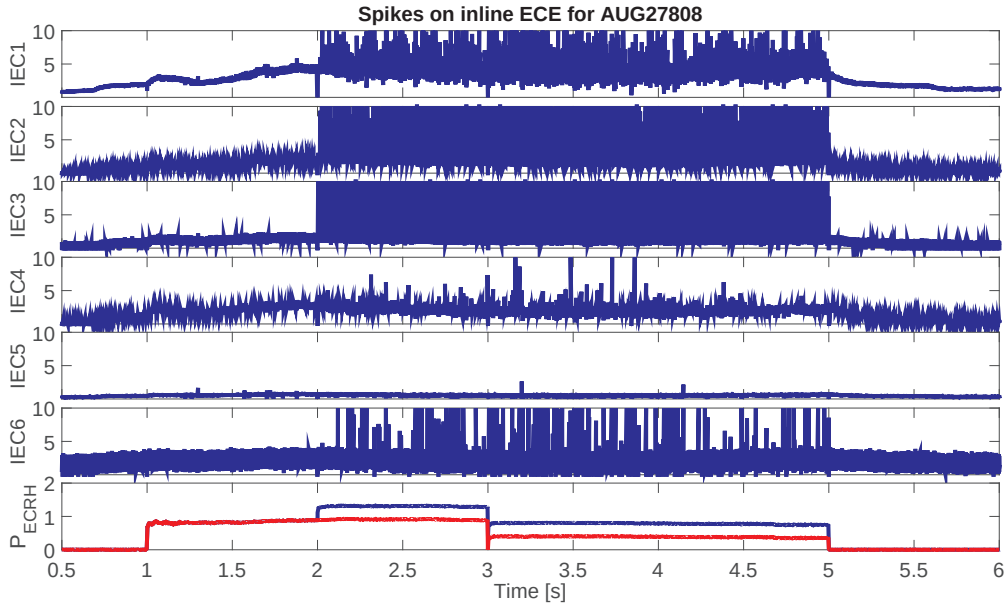

Figure 7. Discharge 27808, in which ECE is measured via FADIS [13]. ECH power, displayed in the bottom graph, is applied via FADIS (blue) and via other transmission lines (red). During ECH power via FADIS, spikes are visible in the six inline ECE measurements.

the inline ECE measurement occurs without an ELM. An example of this is found near 4.28 s. The mechanism for these spikes in absence of ELMs is not yet understood. But the spikes resemble those observed in other devices [25, 26, 27]. At ASDEX Upgrade, the spikes have also been observed with Collective Thomson Scattering (CTS) and are believed to be related to a parametric decay instability that involves the upper hybrid frequency [28, 29]. In between consecutive spikes in figure 8, a time window of about six times the spike duration is found, and therefore about 85 % of the time is still suitable for measurements. The ELM duration for the depicted discharge is on average 0.4 ms.

4. NTM location from inline ECE

Rotating NTMs result in a fluctuating electron temperature, which shows a phase jump at ρ_{NTM}. This is due to the increased temperature for $\rho > \rho_{NTM}$ and temperature decrease for $\rho < \rho_{NTM}$ that occurs in phase with island rotation [30]. The maximum fluctuation is observed at $\rho_{NTM} \pm \frac{w}{2}$, where w is the full width of the magnetic island. These features are employed in multiple detection algorithms (e.g. [12, 31, 8]). Inline ECE measurements at ASDEX Upgrade show a noise level that is comparable to the temperature fluctuation due to a magnetic island. As a result the island fluctuations and their phase cannot be determined directly from the raw signals as was the case for the TEXTOR inline ECE system. Instead, the correlation amplitude and phase with magnetic signals from the Mirnov coils are used to determine the presence and location of an NTM, similar to the method of Reich et al. applied to the data from the standard

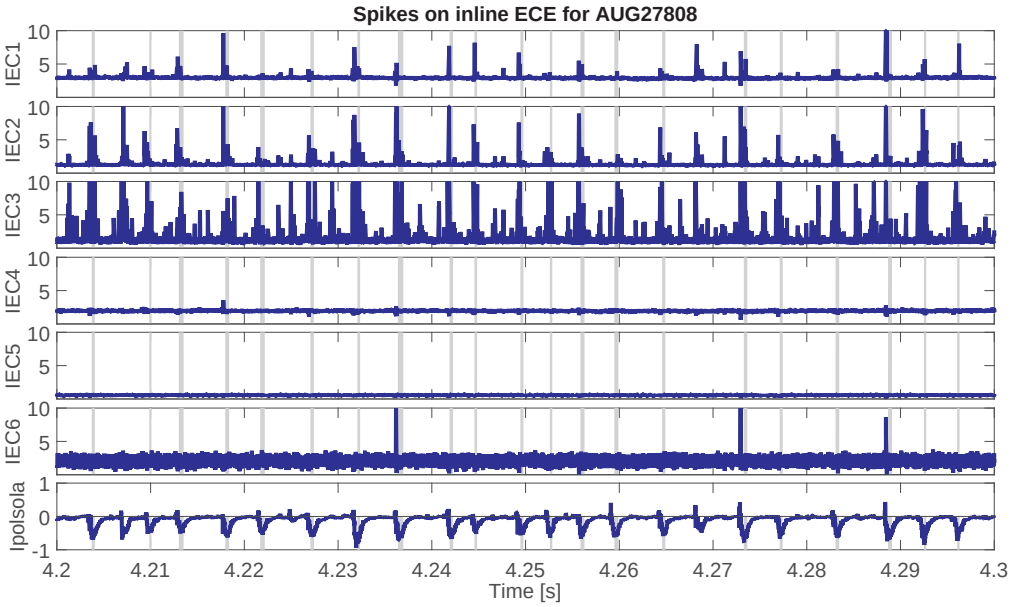

Figure 8. Zoom of discharge 27808 in which spikes are shown on the six inline ECE measurement [13]. The bottom plot shows the divertor current. ELMs are indicated by grey boxes in the background.

ECE diagnostic in ASDEX Upgrade [12]. For completeness, the algorithm for the determination of the correlation amplitude and phase by software lock-in amplification with respect to the magnetic signals, is described in the Appendix. In this section, the resulting correlation amplitude and phase are shown for several NTM discharges.

An example of the correlation amplitude and phase is shown in figure 9. The correlation time of 1 ms is only a factor two larger than the average ELM duration of 0.4 ms, reported in subsection 3.2. Therefore, multiple measurement points show a spread on the amplitudes and phases when the correlation is performed during ELMs. A 9-point median filter is used to smoothen the signal. In the figures presented in the remainder of this section only the results of 9-point median filters, applied to several inline ECE channels, are shown. Therefore, every presented time point is obtained by taking into account a time windows of 9 ms. The median filter ensures that large deviations of the amplitude and phase from the mean value, such as the deviations occurring due to ELMs, are suppressed. Figure 9 also shows a phase drift as a function of time. One would expect the phase difference between magnetic measurements and measurements with inline ECE to remain constant over time. However, for discharge 31978 timing differences in the acquisition units for magnetic measurements and the inline ECE measurements introduce the observed phase drift. While the time difference is partly corrected for, the phase drift shows that the timing correction is not complete.

The results for a slow launcher sweep over the mode location is shown in the next subsection. The correlation amplitude and phase in a case where FADIS is used is

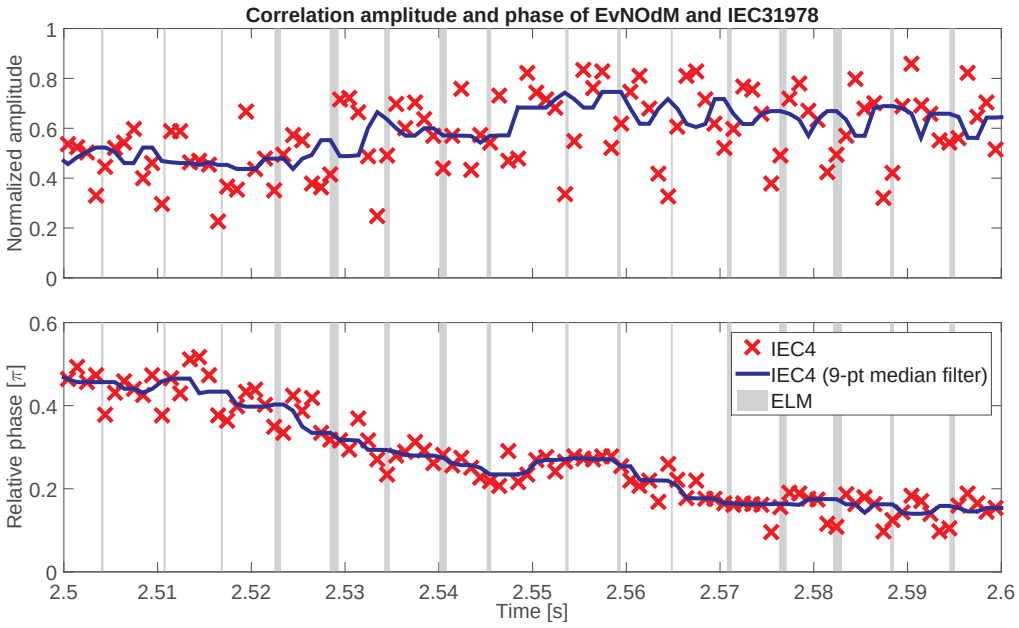

Figure 9. Normalized correlation amplitude (top) and correlation phase (bottom) as a function of time for inline ECE channel 4 for discharge 31978 [13]. The correlation amplitudes and phases, for each 1 ms time window, are shown by red crosses. A 9-point median filter is shown in blue. The time of ELMs is shown by grey boxes.

shown in subsection 4.2. Subsection 4.3 lists the mode crossing times obtained from correlations based on inline ECE and compares this with mode crossing times based on ECE measurements and real-time equilibrium [32, 12]. The applicability of the inline ECE measurements for NTM control is discussed in subsection 4.4.

4.1. Lock-in technique applied to a slow sweep

Figure 10 shows the normalized correlation amplitude and correlation phase as a function of time for inline ECE channels 3, 4, 5, and 6 for discharge 31978. In discharge 31978, inline ECE is measured via a moving launcher that sweeps from an inward position at 3 s, to an outward position at 4.5 s, and then back to the inward location at 6 s. During the inward to outward sweep, ECH is applied via a different launcher at the same flux surface as is used for measurements, but this does not affect the correlation amplitude. The correlation phase shows a slight increase during the discharge, but the most notable feature in the phase are the phase shifts by π near 3.4 s and 5.4 s. These phase shifts occur at the time that the launcher is expected to cross the mode surface, as determined from a mode position based on ECE measurements and the real-time equilibrium [32, 12]. Additionally, the correlation amplitudes are minimal at the moment of the phase jump and maxima in the correlation amplitudes are observed on both sides of the minima. The maxima are due to a measurement at a location $\rho_{NTM} \pm \frac{w}{2}$, while the minima occur near ρ_{NTM}, where the temperature flattened most.

In between 4 s and 5 s, the spread in the relative phase increases. This is the

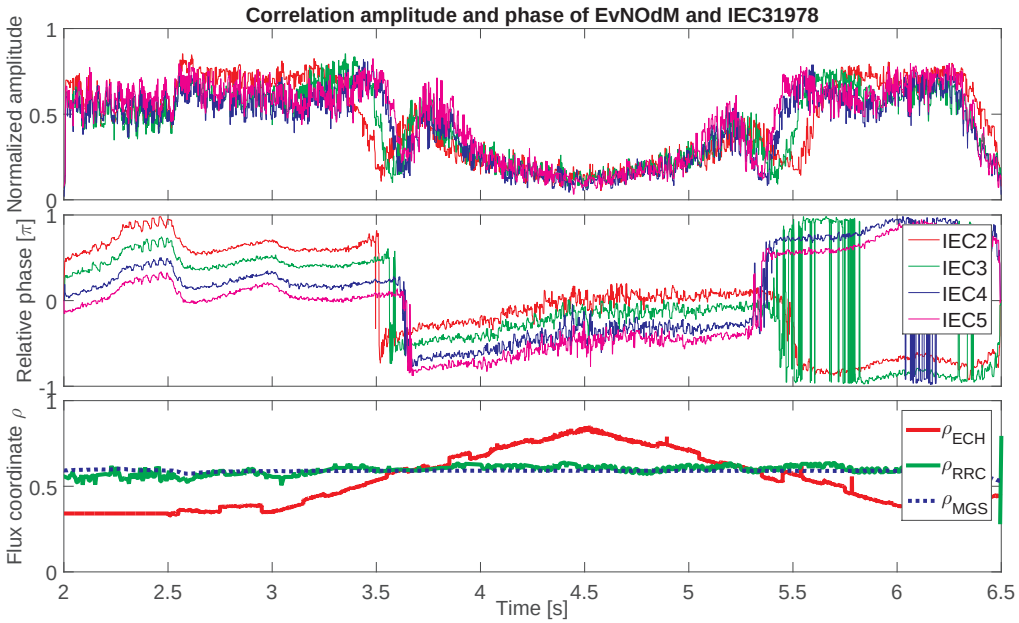

Figure 10. Normalized correlation amplitude (top) and correlation phase (middle) as a function of time for discharge 31978 [13]. The correlation amplitudes and phases, determined with a 9-point median filter based on 1 ms correlation windows, are shown for inline ECE channel 2, channel 3, channel 4, and channel 5 in red, green, blue, and magenta, respectively. In the bottom plot, the mode locations, determined both from ECE measurements ρ_{RRC} and the real-time equilibrium ρ_{MGS} [32, 12], are shown in green and dashed blue, respectively, together with the calculated ECH deposition location from TORBEAM (red). The inline ECE launcher is set for NTM suppression with $\beta = -7.7°$ at a magnetic field of -2.6 T and a plasma current of 1 MA. Phase jumps are visible at the same time as minima in the correlation amplitude are measured. The occurrence of phase jumps and correlation minima depends on the measurement location.

result of a lower correlation amplitude, which also results in a higher inaccuracy of the determined phase. Steps of 2π are visible between 5.5 s and 6.5 s which are due to phase wrapping. A slight drift is visible on all inline ECE channels which is caused by a small timing mismatch between inline ECE and the magnetic signals.

The correlation minima and phase shifts during the slow sweep of the inline ECE measurement locations over the NTM surface allows for the estimation of the NTM crossing time. Similar features have been observed during a slow sweep in discharges 31967 and 31986. In discharge 31967, a 2/1 NTM is present as opposed to a 3/2 NTM in the rest of the presented discharges, but this results in the same features. In Subsection 4.3, the time of mode crossing based on the inline ECE measurements is compared to the mode crossing time based on ECE measurements and the real-time equilibrium.

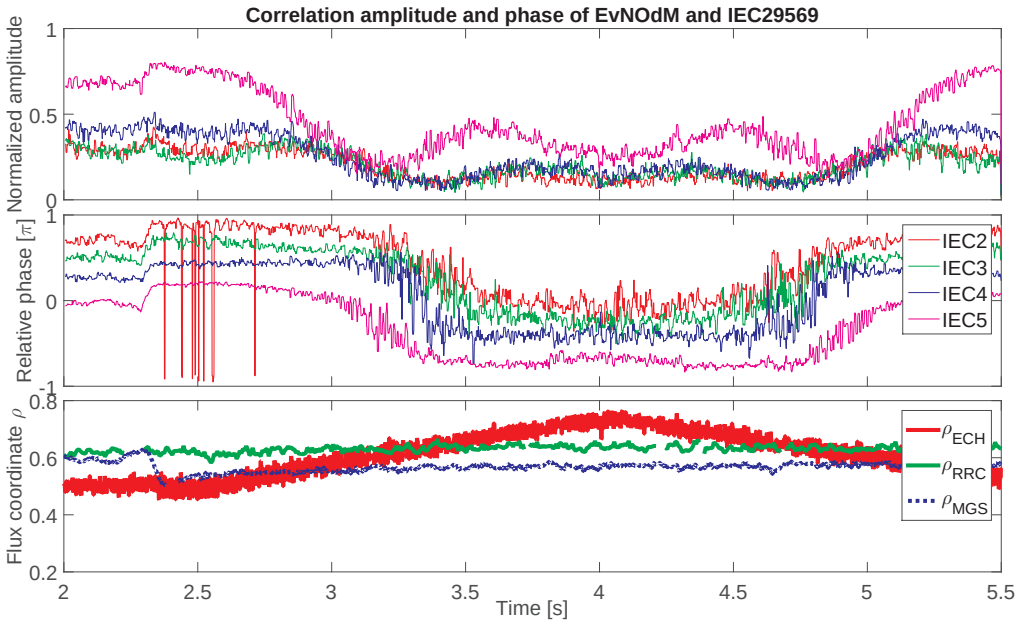

Figure 11. Normalized correlation amplitude (top) and correlation phase (middle) as a function of time for discharge 29569 [13]. The correlation amplitudes and phases, determined with a 9-point median filter based on 1 ms correlation windows, are shown for inline ECE channel 2, channel 3, channel 4, and channel 5 in red, green, blue, and magenta, respectively. In the bottom plot, the mode locations, determined both from ECE measurements ρ_{RRC} and the real-time equilibrium ρ_{MGS} [32, 12], are shown in green and dashed blue, respectively, together with the calculated ECH deposition location from TORBEAM (red). The inline ECE launcher is set for NTM suppression with $\beta = -7.6°$ at a magnetic field of -2.4 T and a plasma current of 1 MA.

4.2. FADIS results

The results presented in the last two subsections are obtained with inline ECE viewing via a separate transmission line. The benefit of inline ECE is largest if it is measured along exactly the same axis as ECH is applied. This is done using FADIS, for instance in discharge 29569, for which correlation results are shown in figure 11. In this case, the same features are found as in subsection 4.1. The minimum in correlation amplitude and the phase jumps are observed at the same time as ECH crosses the mode location based on ECE measurements. The mode position from the real-time equilibrium is not reliable as for discharge 29569 the core of the plasma is not accurately constrained. Such constraints are implemented for discharges 31967 and later [32].

4.3. Mode location from inline ECE

In the previous subsections, it is shown that the time of mode crossing could be determined from the inline ECE measurements. This could be used to assess the mode location. For this purpose, the times of crossing of inline ECE channel 3 and channel 4 (which are on opposite sides of 140 GHz, see subsection 2.1) are determined. The time of crossing is determined both by the minimum in the correlation amplitude and by the

time in between two phase measurements that are shifted by π. The resulting times are indicated in table 2. The average of both crossing times is expected to correspond with ECH crossing the mode location, and is labelled IEC in table 2. Crossing time is chosen as a comparison, because a comparison based on position would require a calculation of the position from the crossing times. This calculation would introduce measurement uncertainties in the magnetic equilibrium into the position calculation, although the magnetic equilibrium is not required to determine the mode location using inline ECE.

The times of crossing based on correlation amplitude and correlation phase are equal, but the crossing of the correlation could be determined with a larger accuracy, as is shown in the table. The crossing times are compared with similar times derived from the crossing of the mode location based on both ECE measurements and the real-time equilibrium with the ECH location [32, 12]. Both are shown in the last two columns of table 2. The error margins for the crossing based on ECE measurements and the real-time equilibrium is influenced by the update time of 0.1 s of the magnetic equilibrium used to determine the ECH location. The crossing times determined with inline ECE are equal to the crossing times determined from ECE and the real-time equilibrium for most discharges. For discharge 31967, there is a small difference between both measurements. The inline ECE crossing time does correspond with a decreased magnetic signal amplitude, which indicates that the inline ECE crossing time is correct.

The determination of the crossing times gives a first indication of the accuracy of inline ECE in relation to other measures for the mode location. However, the mode amplitude or amplitude decrease, as measured by magnetic coils, gives an unbiased measure of whether the ECH location is chosen accurate. If the ECH location could be set based on the inline ECE correlation amplitude and phase, a clear comparison could be made with the standard NTM control loop at ASDEX Upgrade [33, 5].

4.4. Applicability of inline ECE for NTM control

In the previous subsection, it is shown that a mode location could be determined from a slow sweep over the mode location. In contrast to the mode crossing as function of time derived from inline ECE, detection algorithms for the NTM location determine the mode location from a crossing as a function of the flux coordinate ρ [12, 31] or the ECE channel frequencies [8], thereby resolving the mode location without the need for movement of the measurement location.

Figure 4 shows that, due to the tangency of the ECH beam to the 3/2 surface, it is not possible to determine the mode crossing as a function of frequency without launcher movement. At ASDEX Upgrade, the NTM scenario is chosen such that the ECH beam is tangential to the 3/2 flux surface. Therefore, if the maximum deposition is attained at ρ_{NTM}, all channels are measuring inline ECE at $\rho_{IEC,i} > \rho_{NTM}$. This is also illustrated in figure 12, in which the measurement locations for four inline ECE channels are shown as a function of the power deposition location for 140 GHz for discharges 29569 and 31978.

Table 2. Time of mode crossing based on both correlation amplitude and phase [13], compared with crossing times determined based on a crossing of the mode positions from ECE measurements (RRC in table) and the real-time equilibrium (MGS in table) with the ECH location [32, 12]. The average of the crossings based on correlation phase are shown in the column labelled IEC. Crossing times are missing for MGS in discharge 29596, as the real-time equilibrium is not accurate for this discharge.

	Amplitude		Phase				
Discharge	Time IEC3 [s]	Time IEC4 [s]	Time IEC3 [s]	Time IEC4 [s]	Time IEC [s]	Time RRC [s]	Time MGS [s]
29569	3.3 ± 0.1	3.3 ± 0.1	3.41 ± 0.05	3.35 ± 0.05	3.38 ± 0.05	3.3 ± 0.2	-
29569	4.7 ± 0.1	4.7 ± 0.1	4.7 ± 0.1	4.8 ± 0.1	4.8 ± 0.1	4.8 ± 0.2	-
31967	3.48 ± 0.05	3.45 ± 0.05	3.48 ± 0.05	3.46 ± 0.05	3.47 ± 0.05	3.3 ± 0.1	3.3 ± 0.1
31978	3.58 ± 0.05	3.63 ± 0.05	3.56 ± 0.05	3.63 ± 0.05	3.60 ± 0.05	3.7 ± 0.1	3.7 ± 0.1
31978	5.42 ± 0.05	5.4 ± 0.1	5.44 ± 0.05	5.37 ± 0.05	5.41 ± 0.05	5.3 ± 0.2	5.4 ± 0.1
31986	3.9 ± 0.1	4.0 ± 0.1	3.9 ± 0.1	4.02 ± 0.05	3.98 ± 0.08	4.1 ± 0.2	4.1 ± 0.1
31968	5.08 ± 0.05	5.00 ± 0.05	5.11 ± 0.05	5.03 ± 0.05	5.07 ± 0.05	5.0 ± 0.1	5.0 ± 0.1

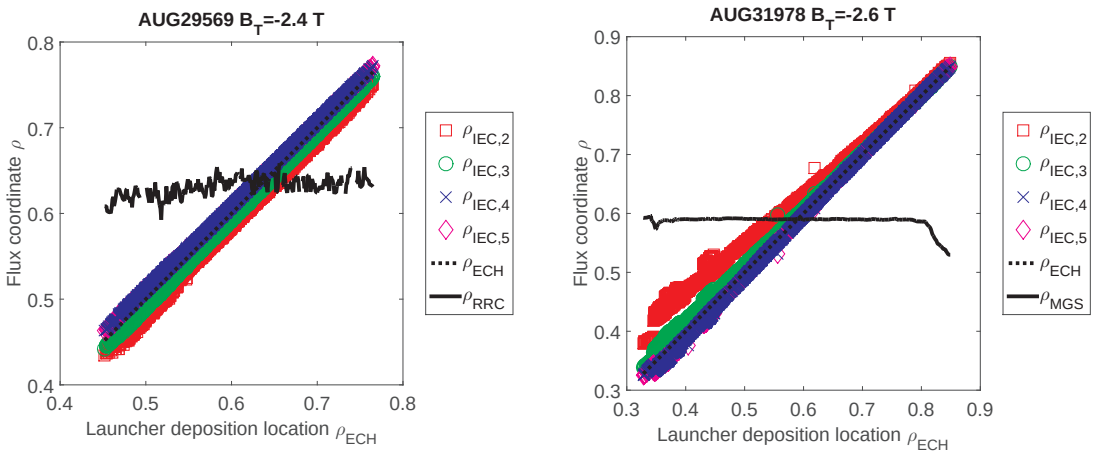

Figure 12. Measurement location of inline ECE channels 2, 3, 4, and 5 as function of the the power deposition location for 140 GHz (dotted black line on top of blue symbols) for discharge 29569 (left), with a magnetic field of -2.4 T, and discharge 31978 (right), with a magnetic field of -2.6 T [13]. The mode location is shown with a solid black line and is obtained from ECE measurements (RRC for 29569) and the real-time equilibrium reconstruction (MGS for 31978). The inline ECE launcher is set for NTM suppression with $\beta = -7.6°$ for 29569 and $\beta = -7.7°$ for 31978, respectively. Note that $\rho_{IEC,4}$ overlaps $\rho_{IEC,5}$ for most data points as both channels measure at the same flux surface (see also figure 4).

For both discharges in figure 12, inline ECE channel 5 is overlapped by inline ECE channel 4. In both cases only a limited part of the plasma is covered by the four depicted inline ECE channels and channels 4 and 5 are both close to the ECH deposition location. For discharge 31978 (right), all channels are positioned such that $\rho_{ECH} \leq \rho_{IEC,i}$. Therefore, the NTM is not visible for $\rho_{ECH} > \rho_{NTM}$. Contrary to discharge 31978, discharge 29569 shows that over the whole range the inline ECE channels cover only a limited region with an ordering of the measurements like $\rho_{IEC,5} \approx \rho_{IEC,4} > \rho_{ECH} > \rho_{IEC,3} > \rho_{IEC,2}$. Note that the different ordering of the inline ECE channels in terms of $\rho_{IEC,i}$ is due to the different magnetic fields: for discharge 29569 $B_T = -2.4$ T, which implies that the ECH resonance is on the high field side, while for discharge 31978 with $B_T = -2.6$ T the resonance is on the low field side. Both for a magnetic field of -2.6 T and a magnetic field of -2.4 T, it is therefore noted that the coverage of the inline ECE channels is not symmetric around the deposition location covering only a limited region. As a consequence, the NTM location is likely to move out of view of the inline ECE channels. This hampers the detection of $\rho_{ECH} = \rho_{NTM}$, because in this case all channels are close to the island resulting in small correlation amplitudes and larger spreads in correlation phase.

Therefore, from a single time point it is only possible to determine the mode location if there is sufficient coverage of ρ using the inline ECE channels for both $\rho_{IEC,i} < \rho_{NTM}$ and $\rho_{IEC,i} > \rho_{NTM}$ for $\rho_{ECH} = \rho_{NTM}$, which is not achieved for both discharges shown in figure 12. However, the mode location can be determined using a launcher sweep. During a sweep over ρ_{NTM}, a phase shift and an amplitude minimum is observed. The phase signal could also be used further away from the island to determine which direction the ECH launcher should be moved, as it shows a similar phase at the start and end of discharges 31978 (figure 10) and 29569 (figure 11), which only depends on whether $\rho_{ECH} < \rho_{NTM}$. The value of the relative phase depends on the set of magnetic coils that is used for lock-in amplification, but the relative phases are consistent for a given coil set.

Close to the island, one could use a sweep of sufficient amplitude, such that one could either minimize the correlation amplitude or continuously look for the point of phase inversion. For discharge 31978, a sweep between the two correlation maxima around 3.5 s requires a launcher sweep with amplitude ± 0.055 around $\rho_{ECH} = 0.565$. The accuracy requirement for determining ρ_{NTM} determines if such a sweep is a viable solution for NTM control. Alternatively, a model-based estimation of ρ_{NTM} could be made using correlation amplitude and phase from the six inline ECE channels. Apart from information on the mode location, the model would also need knowledge of the launcher and plasma geometry.

5. Towards real-time NTM control with inline ECE

In this paper, inline ECE measurements in ASDEX Upgrade H-mode plasmas are considered for the detection of the NTM location. These measurements are done to

analyze the possibility of real-time control of NTMs using inline ECE. This section considers both how to make a comparison between inline ECE and other techniques more accurate, and presents an outline of an inline ECE control loop for NTMs.

In this paper, the location of the inline ECE measurement is determined using TORBEAM, by approximating the emission location with the power deposition location. This approximation is only valid for a constant temperature in the power deposition region and a constant ratio between the emission volume and flux surface volume. The accuracy could be improved by using an EC emission code, such as NOTEC [34], which would need to be adapted to the ASDEX Upgrade launcher locations and angles. Furthermore, Denk *et al* provide a framework suitable to calculate the birthplace distribution of observed intensity, which should be determined for the frequencies measured in the inline ECE channels [22]. The accuracy of the emission location is also determined by the accuracy of the magnetic equilibrium. In this paper, data from the EQI equilibrium is used and as a result steps in the position of maximum power deposition are visible at time points where a different equilibrium is used. A Bayesian approach for determining the magnetic equilibrium for ASDEX Upgrade plasma, which could result in an more accurate equilibrium for determining power deposition locations, is under development for routine use [35].

As is shown in subsection 4.4, inline ECE measurements allow the determination of the mode position from a sweep over ρ_{NTM}. This requires a real-time calculation involving magnetic signals as is done by Reich *et al* [12]. A 9-point median filter is used to suppress the spikes due to ELMs. This technique could also be used in a real-time control algorithm. Alternatively, a model-based approach could be used if there are signals from which spike occurrence can be determined in real-time. A real-time algorithm for determining the crossing with ρ_{NTM} from the correlation signals is not presented in this paper, but such algorithms are common in signal processing [36]. Using a real-time estimate of the crossing location to position the launcher could indicate if the estimate of the crossing location is sufficiently accurate. The mode location could only be determined if the deposition position is varied. Using such a sweep of ρ_{ECH} could be combined with an extremum seeking control technique. An algorithm similar to the algorithm by Wehner *et al* could be used for detecting the minimum in the correlation amplitude [37]. Simulations show that in ITER, contrary to the specific ASDEX Upgrade geometry, the phase jump is detectable without requiring launcher movement [38]. An alternative to a varying deposition location could be the use of a model-based estimation of the ρ_{NTM}. In this case the six correlation amplitudes and six correlation phases are compared with a model, which incorporates information about the mode location that is to be estimated, but which also contains information about the launcher and plasma geometry.

6. Conclusions

In this paper, the inline ECE set-up at ASDEX Upgrade is presented. This set-up contains a six-channel radiometer of which the measurement location could be varied during a discharge. Using FADIS, an inline ECE measurement is possible while simultaneously applying ECH via the same launcher. Thereby a more reactor-relevant implementation of inline ECE is demonstrated.

Interpretation of the measurement results is facilitated by the TORBEAM code. A common feature that is observed in many discharges are spikes that are visible on the measurement channels. The spikes are most likely related to ELMs and show similarities with other high-intensity microwave signals [25, 26, 27, 28, 29].

The lock-in amplification technique, as introduced by Reich *et al* [12], is used to determine correlation amplitude and phase of the inline ECE signals with respect to a magnetic signal. An estimate of the mode location could be made based on a slow sweep of the launcher. This estimation is not hampered by the spikes on the inline ECE measurements.

The time of mode crossing can be determined by a sweep over the mode location with sufficient amplitude. In contrast to other inline ECE NTM control experiments, the mode position could not be determined from a phase jump as a function of the ECE channel frequency. This is due to the specific design of the ASDEX Upgrade ECH system, in which the ECH beam is tangential to the NTM flux surface in order to optimize the local driven current density. As a consequence, the inline ECE measurements show only a limited radial coverage making it more difficult to identify the mode location from the phase jump. This holds in particular when the ECH deposition on the NTM surface coincides with the tangency point of the beam such that $\rho_{IEC,i} > \rho_{ECH} = \rho_{NTM}$. At ASDEX Upgrade, NTM control using inline ECE could be done by using a varying deposition position, which could use an extremum seeking controller. Alternatively, one could also use a model-based estimation of ρ_{NTM} on the basis of the correlation amplitudes and phases for the six inline ECE channels. We note however, that to determine the beam steering the controller may only need to know whether $\rho_{ECH} < \rho_{NTM}$ or $\rho_{ECH} > \rho_{NTM}$, which can be determined uniquely from the correlation phases of the six inline ECE channels, even when ρ_{NTM} is not in sight of the inline ECE system.

Acknowledgments

The work presented in this paper would not have been possible without the technical support of Herr Grünwald, Herr Monaco, Herr Schrepfer, Herr Schütz, Dr. Schubert, Gerben Kaas, and Bob Krijger. The Max Planck Institut für Plasmaphysik Garching is kindly acknowledged for the experimental support and for making the ASDEX Upgrade tokamak available for the inline ECE experiments. This project was carried out with financial support from NWO and the ITER-NL programme. The work has been carried

out within the framework of the EUROfusion Consortium and has received funding from the Euratom research and training programme 2014-2018 under grant agreement No 633053. The views and opinions expressed herein do not necessarily reflect those of the European Commission.

Appendix

Inline ECE measurements at ASDEX Upgrade show a noise level that is comparable to the temperature fluctuation due to a magnetic island. The temperature fluctuations due to the magnetic island could only be distinguished using a Fourier transform of the measurement data, which indicates that the mode is present, but only at a low signal-to-noise level. By means of lock-in amplification, the island fluctuations can be distinguished [12]. Reich *et al* use a correlation between ECE signals and magnetic signals that are both sampled in the same data acquisition unit. The inline ECE measurements are acquired by a data acquisition unit, that is set-up solely for the inline ECE measurements. Consequently, magnetic signals are sampled by a different unit and need to be interpolated to the inline ECE time basis before a correlation could be done. The interpolation should preserve the fluctuating nature of the magnetic signals due to the NTM and should not amplify the noise. This is achieved by processing the magnetic data by a phase locked loop (PLL) such that the phase of the rotation is obtained. The phase signal $\xi(t)$ is interpolated and the sine $s\left(t_{IEC}\right) = \sin\left(\xi(t_{IEC})\right)$ and cosine $c\left(t_{IEC}\right) = \cos\left(\xi(t_{IEC})\right)$ components are calculated on the time instants t_{IEC} of the inline ECE signals. For a selected number of discharges, a magnetic signal $m(t_{IEC})$ is sampled with the inline ECE data acquisition unit and in these discharges $s\left(t_{IEC}\right) = m(t_{IEC})$ and $c\left(t_{IEC}\right)$ is provided by a Hilbert transform of $s\left(t_{IEC}\right)$.

In this way, the correlation amplitude and phase, which are determined by software lock-in amplification with respect to magnetic signals, is obtained as follows. The normalized correlation amplitude $A(t, j_{ch})$ and correlation phase $P(t, j_{ch})$ at time t for inline ECE channel j_{ch} are calculated using

$$\begin{aligned}
C(t, j_{ch}) &= \frac{1}{N}\sum_{i=1}^{N} V_{IEC}\left(t + i\mathrm{d}t, j_{ch}\right) c\left(t + i\mathrm{d}t\right) \\
S(t, j_{ch}) &= \frac{1}{N}\sum_{i=1}^{N} V_{IEC}\left(t + i\mathrm{d}t, j_{ch}\right) s\left(t + i\mathrm{d}t\right) \\
A_{pha}(t, j_{ch}) &= \frac{1}{2N}\sum_{i=1}^{N} \left[C^2\left(t + i\mathrm{d}t, j_{ch}\right) + S^2\left(t + i\mathrm{d}t, j_{ch}\right)\right] \\
A_{IEC}(t, j_{ch}) &= \frac{1}{N}\sum_{i=1}^{N} V_{IEC}^2\left(t + i\mathrm{d}t, j_{ch}\right) \\
A(t, j_{ch}) &= \sqrt{\frac{C^2(t, j_{ch}) + S^2(t, j_{ch})}{A_{IEC}(t, j_{ch}) A_{pha}(t, j_{ch})}} \\
P(t, j_{ch}) &= \arctan\left(\frac{S(t, j_{ch})}{C(t, j_{ch})}\right)
\end{aligned}, \qquad (1)$$

where $V_{IEC}(t, j_{ch})$ is the measurement of inline ECE channel j_{ch} at time t, $N = 400$ for a correlation length of 1 ms with an inline ECE sampling rate of $f_s = 400$ kHz, and $\mathrm{d}t = \frac{1}{f_s}$.

References

[1] T. C. Hender, et al. Progress in the ITER Physics Basis Chapter 3: MHD stability, operational limits and disruptions. *Nuclear Fusion*, 47(6):S128, 2007.

[2] R. J. La Haye. Neoclassical tearing modes and their control. *Physics of Plasmas (1994-present)*, 13(5):055501, 2006.

[3] R. Prater. Heating and current drive by electron cyclotron waves. *Physics of Plasmas*, 11(5):2349–2376, 2004.

[4] M. Maraschek. Control of neoclassical tearing modes. *Nuclear Fusion*, 52(7):074007, 2012.

[5] J. Stober, L. Barrera, K. Behler, A. Bock, A. Buhler, H. Eixenberger, L. Giannone, W. Kasparek, M. Maraschek, A. Mlynek, F. Monaco, E. Poli, C.J. Rapson, M. Reich, M. Schubert, W. Treutterer, D. Wagner, and H. Zohm. Feedback-controlled NTM stabilization on ASDEX Upgrade. *EPJ Web of Conferences*, 87:02017, 2015.

[6] D. A. Humphreys, J. R. Ferron, R. J. La Haye, T. C. Luce, C. C. Petty, R. Prater, and A. S. Welander. Active control for stabilization of neoclassical tearing modes. *Physics of Plasmas (1994-present)*, 13(5):056113, May 2006.

[7] E. Kolemen, A. S. Welander, R. J. La Haye, N. W. Eidietis, D. A. Humphreys, J. Lohr, V. Noraky, B. G. Penaflor, R. Prater, and F. Turco. State-of-the-art neoclassical tearing mode control in DIII-D using real-time steerable electron cyclotron current drive launchers. *Nuclear Fusion*, 54(7):073020, 2014.

[8] B. A. Hennen, E. Westerhof, P. W. J. M. Nuij, J. W. Oosterbeek, M. R. de Baar, W. A. Bongers, A. Bürger, D. J. Thoen, M. Steinbuch, and the TEXTOR Team. Real-time control of tearing modes using a line-of-sight electron cyclotron emission diagnostic. *Plasma Physics and Controlled Fusion*, 52(10):104006, 2010.

[9] E. Westerhof, E. Farshi, J. A. Hoekzema, W. Bongers, O. G. Kruijt, J. W. Oosterbeek, and J. Scholten. A GENERIC METHOD FOR CONTROLLED ECRH/ECCD LOCALISATION. In *EC-13 Joint workshop on ECE and ECRH*, page 357, Nizhny Novgorod, Russia, 2004.

[10] J. W. Oosterbeek, A. Bürger, E. Westerhof, M. R. de Baar, M. A. van den Berg, W. A. Bongers, M. F. Graswinckel, B. A. Hennen, O. G. Kruijt, J. Thoen, R. Heidinger, S. B. Korsholm, F. Leipold, and S. K. Nielsen. A line-of-sight electron cyclotron emission receiver for electron cyclotron resonance heating feedback control of tearing modes. *Review of Scientific Instruments*, 79(9):093503, 2008.

[11] W. A. Bongers, W. Kasparek, N. Doelman, R. van den Braber, H. van den Brand, F. Meo, M. R. de Baar, F.J. Amerongen, A. J. H. Donné, B. S. Q. Elzendoorn, V. Erckmann, A. P. H. Goede, L. Giannone, G. Grünwald, F. Hollman, G. Kaas, B. Krijger, G. Michel, L. Lubyako, F. Monaco, F. Noke, M. Petelin, B. Plaum, F. Purps, J. G. W ten Pierik, C. Schüller, J. W. Slob, J. K. Stober, H. Schütz, D. Wagner, E. Westerhof, D. M. S. Ronden, teams at the contributing institutes, and the ASDEX Upgrade Team. Commissioning of inline ECE system within waveguide based ECRH transmission systems on ASDEX upgrade. *EPJ Web of Conferences*, 32:03006, 2012.

[12] M. Reich, A. Bock, M. Maraschek, and the ASDEX Upgrade Team. NTM Localization by Correlation of T_e and dB/dt. *Fusion Science and Technology*, 61(4):309–313, 2012a.

[13] H. van den Brand. Modelling and measurements for control of magnetic instabilities in tokamak plasmas. *PhD Thesis Technical university Eindhoven*, 2016.

[14] D. Wagner, J. Stober, F. Leuterer, F. Monaco, S. Müller, M. Münich, C. J. Rapson, M. Reich, M. Schubert, H. Schütz, W. Treutterer, H. Zohm, M. Thumm, T. Scherer, A. Meier, G. Gantenbein, J. Jelonnek, W. Kasparek, C. Lechte, B. Plaum, T. Goodman, A. G. Litvak,

G. G. Denisov, A. Chirkov, V. Zapevalov, V. Malygin, L. G. Popov, V. O. Nichiporenko, V. E. Myasnikov, E. M. Tai, E. A. Solyanova, S. A. Malygin, and the ASDEX Upgrade Team. Status, Operation, and Extension of the ECRH System at ASDEX Upgrade. *Journal of Infrared, Millimeter, and Terahertz Waves*, 37(1):45–54, 2015a.

[15] W. Kasparek, R. van den Braber, N. Doelman, E. Fritz, V. Erckmann, F. Hollmann, G. Michel, F. Noke, F. Purps, W. Bongers, B. Krijger, M. Petelin, L. Lubyako, A. Bruschi, and ECRH Groups at IPP Greifswald and IPF Stuttgart. High-Power Performance of a Resonant Diplexer for Advanced ECRH. *Fusion Science and Technology*, 59(4):729–741, May 2011.

[16] H. J. Hartfuss, T. Geist, and M. Hirsch. Heterodyne methods in millimetre wave plasma diagnostics with applications to ECE, interferometry and reflectometry. *Plasma Physics and Controlled Fusion*, 39(11):1693, November 1997.

[17] N. Doelman, R. van den Braber, W. Kasparek, V. Erckmann, W. Bongers, B. Krijger, J. Stober, E. Fritz, B. Dekker, W. Klop, F. Hollmann, G. Michel, F. Noke, F. Purps, M. de Baar, M. Maraschek, F. Monaco, S. Müller, H. Schütz, D. Wagner, the ASDEX Upgrade Team, and other teams at the contributing institutes. Controlled Mirror Motion System for Resonant Diplexers in ECRH Applications. *EPJ Web of Conferences*, 32:04005, 2012.

[18] W. Kasparek, B. Plaum, C. Lechte, Z. Wu, H. Wang, M. Maraschek, J. Stober, D. Wagner, M. Reich, M. Schubert, G. Grünwald, F. Monaco, S. Müller, H. Schütz, V. Erckmann, N. Doelman, R. van den Braber, W. Klop, H. van den Brand, W. Bongers, B. Krijger, M. Petelin, E. Koposova, L. Lubyako, A. Bruschi, and K. Sakamoto. Development of Resonant Diplexers for high-power ECRH – Status, Applications, Plans. *EPJ Web of Conferences*, 87:04010, 2015.

[19] W. A. Bongers, A. P. H. Goede, E. Westerhof, J. W. Oosterbeek, N. J. Doelman, F. C. Schuller, M. R. De Baar, W. Kasparek, W. Wubie, D. Wagner, J. Stober, and the TEXTOR Team. MAGNETIC ISLAND LOCALIZATION FOR NTM CONTROL BY ECE VIEWED ALONG THE SAME OPTICAL PATH OF THE ECCD BEAM. *FUSION SCIENCE AND TECHNOLOGY*, 55(2):188–203, February 2009.

[20] D. Wagner, W. Bongers, W. Kasparek, F. Leuterer, F. Monaco, M. Münich, H. Schütz, J. Stober, M. Thumm, and H. van den Brand. A Multifrequency Notch Filter for Millimeter Wave Plasma Diagnostics based on Photonic Bandgaps in Corrugated Circular Waveguides. *EPJ Web of Conferences*, 87:04012, 2015b.

[21] E. Poli, A. G. Peeters, and G. V. Pereverzev. TORBEAM, a beam tracing code for electron-cyclotron waves in tokamak plasmas. *COMPUTER PHYSICS COMMUNICATIONS*, 136(1-2):90–104, May 2001.

[22] S. S. Denk, R. Fischer, H.M. Smith, P. Helander, O. Maj, E. Poli, J. Stober, U. Stroth, W. Suttrop, E. Westerhof, M. Willensdorfer, and the ASDEX Upgrade Team. Analysis of electron cyclotron emission with extended electron cyclotron forward modeling. *Plasma Physics and Controlled Fusion*, 60:105010, 2018.

[23] R. Fischer, C. J. Fuchs, B. Kurzan, W. Suttrop, E. Wolfrum, and the ASDEX Upgrade Team. Integrated Data Analysis of Profile Diagnostics at ASDEX Upgrade. *Fusion Science and Technology*, 58(2):675–684, October 2010.

[24] A. W. Leonard. Edge-localized-modes in tokamaks. *Physics of Plasmas (1994-present)*, 21(9):090501, 2014.

[25] E. Westerhof, S. K. Nielsen, J. W. Oosterbeek, M. Salewski, M. R. De Baar, W. A. Bongers, A. Bürger, B. A. Hennen, S. B. Korsholm, F. Leipold, D. Moseev, M. Stejner, and D. J. Thoen. Strong Scattering of High Power Millimeter Waves in Tokamak Plasmas with Tearing Modes. *Physical Review Letters*, 103(12):125001, September 2009.

[26] S. J. Freethy, K. G. McClements, S. C. Chapman, R. O. Dendy, W. N. Lai, S. J. P. Pamela, V. F. Shevchenko, and R. G. L. Vann. Electron Kinetics Inferred from Observations of Microwave Bursts During Edge Localized Modes in the Mega-Amp Spherical Tokamak. *Physical Review Letters*, 114(12):125004, March 2015.

[27] B. J. Tobias, M. E. Austin, J. E. Boom, I. G. J. Classen, C. W. Domier, N. C. Luhmann,

R. Nazikian, and L. Yu. Intense millimeter wave radiation from the H-mode pedestal in DIII-D at ITER relevant collisionality. In *39th EPS Conference on Plasma Physics*, page P4.019, 2012.

[28] S. K. Nielsen, M. Salewski, E. Westerhof, W. Bongers, S. B. Korsholm, F. Leipold, J. W. Oosterbeek, D Moseev, and M. S. Pedersen. Experimental characterization of anomalous strong scattering of mm-waves in TEXTOR plasmas with rotating islands. *Plasma Physics and Controlled Fusion*, 55(11), 2013.

[29] S. K. Nielsen, W. Bongers, S. Fietz, A. S. Jacobsen, S. B. Korsholm, F. Leipold, D. Moseev, J. Rasmussen, M. Salewski, M. Schubert, M. S. Pedersen, J. Stober, D. Wagner, and E. Westerhof. Strong scattering of mm-waves in tokamaks. *Proceedings of the 9th International Workshop "Strong Microwaves and Terahertz Waves: Sources and Applications"*, 2014.

[30] R. Fitzpatrick. Helical temperature perturbations associated with tearing modes in tokamak plasmas. *Physics of Plasmas*, 2(3):825–838, 1995.

[31] J. Berrino, E. Lazzaro, S. Cirant, G. D'Antona, F. Gandini, E. Minardi, and G. Granucci. Electron cyclotron emission temperature fluctuations associated with magnetic islands and real-time identification and control system. *Nuclear Fusion*, 45(11):1350, 2005.

[32] L. Giannone, R. Fischer, P. J. McCarthy, T. Odstrcil, I. Zammuto, A. Bock, G. Conway, J. C. Fuchs, A. Gude, V. Igochine, A. Kallenbach, K. Lackner, M. Maraschek, C. Rapson, Q. Ruan, K. H. Schuhbeck, W. Suttrop, and L. Wenzel. Improvements for real-time magnetic equilibrium reconstruction on ASDEX Upgrade. *Fusion Engineering and Design*, 100:519–524, November 2015.

[33] M. Reich, R. Bilato, U. Mszanowski, E. Poli, C. Rapson, J. Stober, F. Volpe, and R. Zille. Real-time beam tracing for control of the deposition location of electron cyclotron waves. *Fusion Engineering and Design*, 100:73–80, 2015.

[34] R. M. J. Sillen, M. A. F. Allaart, W. J. Goedheer, and A. Kattenberg. NOTEC: A CODE TO SIMULATE ELECTRON CYCLOTRON EMISSION SPECTRA OF PLASMAS WHICH INCLUDE NON-THERMAL POPULATIONS. Rijnhuizen Report 86-165, FOM Institute for Plasma Physics, Nieuwegein, The Netherlands, 1987.

[35] R. Fischer, A. Bock, M. Dunne, and J. C. Fuchs. Coupling of the Flux Diffusion Equation with the Equilibrium Reconstruction at ASDEX Upgrade. *Fusion Science and Technology*, 69(2), 2016.

[36] M. Basseville. Detecting changes in signals and systems—A survey. *Automatica*, 24(3):309–326, May 1988.

[37] W. Wehner and E. Schuster. Control-oriented modelling for neoclassical tearing mode stabilization via minimum-seeking techniques. *Nuclear Fusion*, 52(7):074003, 2012.

[38] H. van den Brand, M. R. de Baar, N. J. Lopes Cardozo, and E. Westerhof. ECE for NTM control on ITER. *EPJ Web of Conferences*, 32:6, 2012b.